Differential GNSS for Ranging and Synchronization Between Lunar Orbiters: Impact of Large Baselines and Relative Dynamics

Differential GNSS for ranging and synchronization between lunar orbiters: Impact of large baselines and relative dynamics

Anaïs Delépaut, Alex Minetto, Fabio Dovis
Politecnico di Torino
Dept. of Electronics and Telecommunications (DET)
Turin, Italy
{anais.delepaut, alex.minetto, fabio.dovis}@polito.it

***Abstract*—As lunar exploration progresses, autonomous spacecraft navigation is becoming critical. Global Navigation Satellite System (GNSS) signals provide a valuable alternative to traditional ground-based systems, offering real-time navigation for lunar orbiters. NASA's LuGRE initiative recently demonstrated GNSS signals reception at 432,384 km from Earth, proving its feasibility despite challenges such as low power levels and poor geometry. These limitations justify the need for augmentation strategies to extend GNSS usability in the Space Service Volume (SSV) and potentially support future lunar navigation systems. This study investigates cooperation between lunar orbiters via Differential GNSS (DGNSS) where missions are assumed to exchange pseudorange and Doppler measurements to estimate their Inter-Spacecraft Ranges (ISR). A key challenge is the asynchronous nature of pseudorange data caused by clock biases because of the large dynamics characterizing such scenario. Therefore, this work provides an assessment of a time-extrapolation technique used to mitigate these offsets and then evaluates its impact on the ISR estimation process using simulated data. The findings provide insights into DGNSS as a potential augmentation solution, supporting the roadmap towards a robust lunar navigation architecture.**

***Index Terms*—DGNSS ranging, GNSS in space, lunar missions, asynchronous pseudoranges combination**

I. Introduction

As the second wave of lunar exploration gains momentum, the development of navigation solutions for spacecrafts visiting the Moon is in the spotlight. Traditional space navigation methods, which have largely depended on ground-based systems such as the Deep Space Network (DSN), are being reevaluated in favour of more autonomous solutions [1]. Among these, Global Navigation Satellite System (GNSS) signals have emerged as a promising tool, providing real-time navigation capabilities for lunar orbiters.

In recent years, significant advancements have been made in applying GNSS beyond Earth's orbit, even though these signals were originally designed for terrestrial use. Spacecrafts in lunar orbit face challenges such as signal attenuation and limited satellite visibility, but modern developments in GNSS technology, including enhanced receiver sensitivity [2], improved signal processing algorithms [3], and access to multi-constellation GNSS such as Galileo and GPS have made continuous onboard navigation at such altitudes more realistic. Recognizing this potential, National Aeronautics and Space Administration (NASA), in collaboration with Italian Space Agency (ASI), has just set a new record by picking up Galileo and Global Positioning System (GPS) signals at a distance of $432384\,\mathrm{km}$ from Earth with their Lunar GNSS Receiver Experiment (LuGRE) [4], [5] and the European Space Agency (ESA) is set to follow with their Navimoon initiative soon to be flown on the Lunar Pathfinder mission [2], [6]. These innovations would enable spacecrafts to reduce their reliance on ground-based tracking systems, offering real-time positioning, velocity determination, and time synchronization. As a result, GNSS-based navigation has become an attractive solution for future lunar missions, which demand greater autonomy and precision. However, relying solely on GNSS signals in lunar orbit presents limitations due to poor signal geometry at such distances [1]. The clustering of GNSS satellites near Earth's horizon leads to suboptimal Geometric Dilution of Precision (GDOP), degrading the precision of the positioning solution [7]. While GNSS can support autonomous navigation, it may not be sufficient to meet the requirements of precise operations required for upcoming missions. With over 400 planned lunar missions by space agencies and private companies in the next two decades and the success of inter GNSS users collaboration to increase the individual performance of GNSS users in terrestrial applications, the present context calls for testing inter-mission cooperation between lunar users to ultimately improve the individual GNSS performance while keeping the navigation infrastructure costs low [8].

By sharing multi-constellation, multi-frequency pseudorange and Doppler shift measurements, spacecrafts can generate additional ranging measurements with neighbouring space missions [9]. These techniques fall under the category of Differential GNSS (DGNSS). Exploiting neighbouring lunar missions as anchors of opportunity would allow to improve the geometry of the sources involved in the creation of the onboard navigation solution while leveraging on the resources already planned for the Moon [10]. However, because each mission will have their own local clock onboard, the set of pseudorange measurements made onboard of each cooperating

GNSS receiver will be asynchronous. An important step in the process of DGNSS inter-user range estimation hence consists in extrapolating the measurements of the anchors of opportunity to the timestamps of the target GNSS receiver. This technique was successfully used for cooperation among GNSS users on earth [11]. However, the dynamics inherent to space users are significantly different than terrestrial ones and could impact the final performance of DGNSS inter-user ranging [9].

This measurement time extrapolation technique relies on a product between the GNSS Doppler shift measurements of the space user and the individual clock bias estimates of both cooperating users. The Doppler measurements between lunar orbiters and GNSS satellites reaching values up to 10 times larger than in the case of terrestrial applications, the noise variance characterizing the clock bias estimates may degrade even more the extrapolated pseudorange estimation quality. Moreover, this technique assumes that the Doppler shifts stay constant over the duration in which the pseudorange set is being extrapolated. The space GNSS users dynamics varying faster when compared to those of terrestrial ones, this assumption may not anymore be taken for granted in space. Hence, the present paper aims to investigate these aspects.

In particular, it assumes the scenario case where both the Lunar Pathfinder and the Volatile and Mineralogy Mapping Orbiter (VMMO) missions are flying around the Moon and exchanging their pseudorange and Doppler measurements made from Galileo and GPS systems. It assesses the ranging and timing errors associated to DGNSS techniques. Finally, the effect of pseudorange time-extrapolation error on the performance of inter GNSS users ranging in space is investigated.

The paper is structured as follows: section II describes the fundamentals of the GNSS-based baseline estimation, section III describes the simulation blocks used to perform this analysis and the considered space scenario used to assess the effect of asynchronous pseudorange measurements on DGNSS ranging in space. Finally, section IV presents the results achieved with this environment and analyzes the potential performance of inter-agent GNSS ranging in space with asynchronous measurements.

II. DGNSS RANGING IN SPACE

Relative ranging radio technologies allow the computation of the distance $d_{ij,k}$ between two moving objects i and j, at a given time instant t_k. A subgroup of those technologies directly provide an estimate of $d_{ij,k}$ by means of signal Time of Flight (ToF) or Round Trip Time (RTT). DGNSS techniques instead first indirectly estimate the displacement vector $\mathbf{d}_{ij,k}$ between the two users positions $\mathbf{x}_{i,k}$ and $\mathbf{x}_{j,k}$, a.k.a. *baseline vector*,

$$\mathbf{d}_{ij,k} = \begin{bmatrix} \Delta x_{ij,k} & \Delta y_{ij,k} & \Delta z_{ij,k} \end{bmatrix}, \tag{1}$$

and subsequently estimate the range by taking the Euclidean norm of (1). In [12], different GNSS-based ranging techniques are presented and applied to terrestrial applications. The most straighforward called Absolute Positions Differencing (APD) is based on the direct difference of the GNSS estimated position of both users involved. Many ways exist to estimate the position in the GNSS framework, varying in accuracy and precision. However, the present contribution considers a pseudorange-based Single Point Position (SPP) estimation with an iterative Least Squares (LS) algorithm to keep the focus and understanding on the range estimation algorithms.

The other GNSS-based ranging algorithms are known under the name of DGNSS ranging techniques and rely on the inter-user combination of pseudorange measurements. As the receivers' local clock are asynchronous, the pseudorange measurements of the *aiding user* must be time-extrapolated at the measurement timestamps of the *aided user*. This technique is based on Doppler shifts and is described below.

The inter-user combination of pseudoranges can be done via Single Differences (SD) and Double Differences (DD). However, traditional DGNSS ranging algorithms used in terrestrial applications were shown not to be adequate for a scenario of lunar orbiters due to the invalidity of the parallelism assumption usually taken for granted in terrestrial scenarios, as presented in [9]. The issue is summarized below and the solutions presented in [9] are reported in the presented contribution as they are applied to the studied lunar scenario.

A. Positioning algorithm

As explained in [7], [13], [14], the pseudorange measurements made between GNSS receiver i and satellite s at epoch t_k are affected by various sources of errors and can be decomposed into

$$\rho^s_{i,k} = r^s_{i,k} + b_{i,k} - c \cdot \delta t^s_k + d_{atm,k} + \epsilon^s_{i,k} \tag{2}$$

where $r^s_{i,k}$ is the range between receiver i and satellite s, $b_{i,k} = c \cdot \delta t^r_{i,k}$ is the range offset caused by the receiver's local clock bias $\delta t^r_{i,k}$ with respect to the system timescale, δt^s_k is the modeled part of the satellite clock offset with the system time, which can be partly corrected for, using the values broadcast in the navigation messages (for SPP), as well as a small relativistic correction needed to compensate for the orbital eccentricity, and $d_{atm,k}$ are the atmospheric delays. Finally, $\epsilon^s_{i,k}$ represents the unmodelled errors including receiver noise, multipath signals, orbital errors and other effects as referenced by [15].

The SPP estimate of each user is obtained thanks to an Iterative Least Squares (ILS) estimator, where at each iteration l, the user assumed position $\hat{\mathbf{x}}_{*,k}$ and clock bias $\hat{b}_{*,k}$ are updated based on the linearisation of the pseudorange equation with a Taylor expansion truncated at the first order

$$\begin{aligned} \hat{\mathbf{x}}_{*,k} &= \hat{\mathbf{x}}^{l-1}_{*,k} + \Delta\hat{\mathbf{x}}^{l}_{*,k}, \\ \hat{b}_{*,k} &= \hat{b}^{l-1}_{*,k} + \Delta\hat{b}^{l}_{*,k}, \end{aligned} \tag{3}$$

where $\hat{\mathbf{x}}^{l-1}_{*,k}$ and $\hat{b}^{l-1}_{*,k}$ are the position and bias estimated at the previous iteration $l-1$ for user $*$ (i or j, interchangeably) and $\Delta\hat{\mathbf{x}}^{l}_{*,k}$ and $\Delta\hat{b}^{l}_{*,k}$ are the increments in position and clock bias for the current iteration l and are obtained thanks to

$$\begin{bmatrix} \Delta\hat{\mathbf{x}}^{l}_{*,k} \\ \Delta\hat{b}^{l}_{*,k} \end{bmatrix} = \left(\mathbf{H}^\top\mathbf{H}\right)^{-1}\mathbf{H}^\top\boldsymbol{\Delta\rho}^{l}_{*,k}, \tag{4}$$

where $\mathbf{H}$ is the $N \times 4$ direction cosine matrix estimated from the last iteration estimate of the user position and is made of the *unit steering vectors* to the satellites, $\mathbf{h}^s_*$, [7]. $\boldsymbol{\Delta\rho}^l_{*,k}$ is the pseudorange increment vector $N \times 1$ which has been corrected for the user clock bias and the Signal In Space Error (SISE) as well as the relativistic effects. N represents the number of GNSS satellites involved in the computation and must be at least equal to 4 to solve for the 4 unknowns.

B. Inter-user cooperation

For DGNSS ranging to be performed, the availability of a low-latency communication link between the cooperating users is assumed, also known as Inter-Satellite Link (ISL) in space. In such conditions, a GNSS user called *aiding* can send its GNSS pseudorange and Doppler measurements to the *aided* user, as depicted in Fig. 1. If available, it can also share with the aided user its local position and clock bias estimation. However, DGNSS ranging can also be performed without this information, as justified in section II-D.

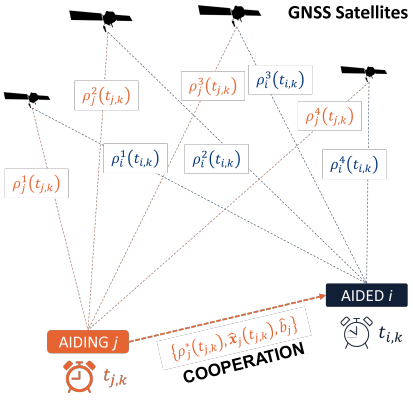

Fig. 1: DGNSS based ranging scenario.

C. Time-extrapolation of the aiding user pseudoranges at the aided user measurements timestamps

Due to their asynchronous clocks, there is a time offset between the measurements of the pair of receivers, defined as $\Delta t_{ij,k} = t_{j,k} - t_{i,k}$, where $t_{*,k}$ is the receiver timestamp associated to a given set of pseudorange measurements after correction of the corresponding receiver clock bias $\delta t^r_{*,k}$ for user $*$ (which denotes the user ID, i or j). For the measurement sets of both users to be coherently combined with one another, they must both be defined at a unique common timestamp. The technique to extrapolate the measurements of the *aiding user* to the *aided user* measurement timestamps, as introduced in [11], is based on the Doppler frequency shift of the *aiding user* j with the satellite s, $\phi^s_j(t_{j,k})$ such that

$$\begin{aligned}\hat{\rho}^s_j(t_{i,k}) &= \rho^s_j(t_{j,k} - \Delta t_{ij,k}) \\ &= \rho^s_j(t_{j,k}) + \Delta t_{ij,k} \cdot \lambda_{f_c} \cdot \phi^s_j(t_{j,k}),\end{aligned} \tag{5}$$

where λ_{f_c} is the wavelength associated to the carrier frequency of the GNSS signals, $0.2549\,\text{m}$ for L5/E5a, being the focus frequency band of the present contribution, given its inherent advantages for spaceborne GNSS users, as discussed in [1].

D. DGNSS ranging and timing techniques

Once the aiding pseudorange measurements received and time-extrapolated, SD and DD combinations can be performed to proceed to the ranging step. In the context of space applications, such range is also called Inter-Spacecraft Range (ISR).

1) Single Differences ranging: A generic SD can be defined between two GNSS receivers, i and j tracking a common satellite s as the difference between synchronous pseudorange measurements

$$\begin{aligned}S^s_{ij,k} &= \rho^s_{j,k} - \rho^s_{i,k} \\ &= \Delta r^s_{ij,k} + \Delta b_{ij,k} + \Delta\epsilon_{ij,k},\end{aligned} \tag{6}$$

where $\Delta b_{ij,k}$ is the difference between the clock biases of the two agents and $\Delta\epsilon_{ij,k}$ is a noise term which aggregates all the uncorrelated errors. In fact, provided that all the measurements are synchronous, SDs allow to cancel the GNSS satellite clock bias and other correlated bias terms affecting pseudorange measurements. Besides the cancellation of correlated error terms, the variance of the uncorrelated errors, such as thermal noise, is increased. These noise contributions are hence aggregated in $\Delta\epsilon_{ij,k}$.

The computation of the baseline vector based on SD is performed through (7), assuming a minimum of 4 visible GNSS satellites common to both users if the differential clock bias $\Delta b_{ij,k}$ is unknown and 3 visible satellites if $\Delta b_{ij,k}$ is considered already known, in which case the column of ones in (7) could be removed.

$$\begin{bmatrix} S^1_{ij,k} \\ S^2_{ij,k} \\ \vdots \\ S^S_{ij,k} \end{bmatrix} \simeq - \begin{bmatrix} \mathbf{h}^1_{i,k} & 1 \\ \mathbf{h}^2_{i,k} & 1 \\ \vdots & \vdots \\ \mathbf{h}^S_{i,k} & 1 \end{bmatrix} \begin{bmatrix} \mathbf{d}_{ij,k} \\ \Delta b_{ij,k} \end{bmatrix} \tag{7}$$

The estimated $\Delta\hat{b}_{ij,k}$ via (7) is referred to *differential clock bias* in the rest of the paper, while $\Delta\hat{b}_{ij,k}$ estimated taking the difference of the individually LS estimated $\hat{b}_{*,k}$ in (3) such that $\Delta\hat{b}_{ij,k} = \hat{b}_{j,k} - \hat{b}_{i,k}$ is referred to *difference of estimated clock biases*, being also a product of the estimation called `APD`, later described in Table I.

2) Double Differences ranging: When the same pair of satellites r and s is visible to both receivers, a DD measurement can be obtained as difference of two SDs:

$$D^{rs}_{ij,k} = S^s_{ij,k} - S^r_{ij,k} = \Delta R^{sr}_{ij,k} + \Sigma_{ij,k}, \tag{8}$$

where S^s_{ij} is a SD computed according to (6) while Σ_{ij} is a random variable collecting residual error contributions that cannot be cancelled due to the non-correlation between the measurements such as multipath, second-order noise components of the receiver front-ends and residual, unmodelled noise contributions [7]. The term ΔR^{sr} can be expressed highlighting the dependency from the baseline vector as:

$$\Delta R^{sr,k} = \left[\mathbf{h}^r_{*,k} - \mathbf{h}^s_{*,k}\right]^T \mathbf{d}_{ij,k}. \tag{9}$$

In order to determine the steering vectors used in (7) and (9), an approximation of the two positions is needed. A GNSS receiver can solve for the aiding position by using the extrapolated aiding pseudorange measurements. By means of this approach, the exchange of the estimated position is not a strict requirement since it can be computed autonomously at the aided receiver.

One difference between SD ranging and DD ranging is that DD ranging cancels out the receivers differential clock bias out of the measurements. Therefore, only the relative distance can be estimated out of this technique. Also, a minimum of 4 commonly visible GNSS satellites are needed in any circumstance for this technique, since one satellite is needed as pivot to construct the DD.

E. Characteristics of a space DGNSS scenario

When dealing with the application of DGNSS in a terrestrial scenario, the relationship in (7) is valid since it is based on a parallelism assumption of the steering vectors of the users with respect to the GNSS satellites [12], [16]–[19]. Under such assumption, the difference in true ranges $\Delta r^s_{ij,k}$ can be approximated by the inner product between the baseline vector $\mathbf{d}_{ij,k}$ and the unit steering vector $\mathbf{h}^s_{i,k}$ or $\mathbf{h}^s_{j,k}$ between either user i or j and the satellite s, i.e.:

$$\Delta r^s_{ij,k} \simeq -\left[\mathbf{h}^s_{*,k}\right]^T \mathbf{d}_{ij,k} \tag{10}$$

However, in a space scenario, the typical distances of a DGNSS scenario involving lunar orbiters and terrestrial GNSS satellites lead the ratio between the baseline and the GNSS user to GNSS satellite to be easily two orders of magnitude larger than for terrestrial applications. The parallelism assumption is therefore not applicable anymore such that a bias is observed when the inter-user range is estimated based on the parallelism assumption for a space scenario. A few solutions thoroughly described in [9] are based on updating the steering vectors used in (7) and (9) depending on the user of which the position estimate is used to build the DGNSS technique design matrix and are defined in Table I. The presented techniques are all based on the measurements defined in (6) and (8), except `APD` that is based on the difference of the solutions defined in (3).

III. Methodology

To investigate a realistic case study, it is crucial for a GNSS receiver to receive signals that are characterized by power levels and Doppler profiles aligned with those received by a GNSS user in lunar orbit from the reference Medium-Earth Orbit (MEO) GNSS constellations. To accomplish this, the constellation propagator tool AGI Systems Tool Kit (STK) is employed to simulate GNSS satellites, model the communication channel with the receiver, and propagate the two users' initial state. During a 4 hours track starting on 09-Nov-2025 00:00:00.000 UTC, the GNSS satellites position time series, the C/N_0 and Doppler shifts of the signals received by the two receivers as well as the users' position time series were collected and logged. These data were then passed to the post-processing stage in Matlab as described in Fig. 2 showing the simulation blocks involved in the simulation.

TABLE I: GNSS ranging and timing techniques according to [9].

Name	Description
`APD`	Direct difference of the GNSS estimated state vectors of both users involved.
`SD` or `DD` $\mathtt{H}_{\mathtt{aided}}$	SD or DD terrestrial DGNSS technique where the aided user position is used to build the steering vectors in (7).
`SD` or `DD` $\mathtt{H}_{\mathtt{aiding}}$	SD or DD terrestrial DGNSS technique where the aiding user position is used to build the steering vectors in (7).
`SD` $\mathtt{H}_{\mathtt{aided,corrected}}$	SD DGNSS technique where the aided user position is used to build the steering vectors in (7) and the pseudoranges measurements were corrected to compensate for the invalidity of the parallelism assumption.
`SD` or `DD` $\mathtt{H}_{\mathtt{sum}}$	SD or DD DGNSS technique where a combination of steering vectors from both users' positions is used in (7) to compensate for the invalidity of the parallelism assumption.
`SD` or `DD` $\mathtt{H}_{\mathtt{ideal}}$	SD or DD DGNSS technique where a steering vector considered as ideal to compensate for the invalidity of the parallelism assumption is used in (7).

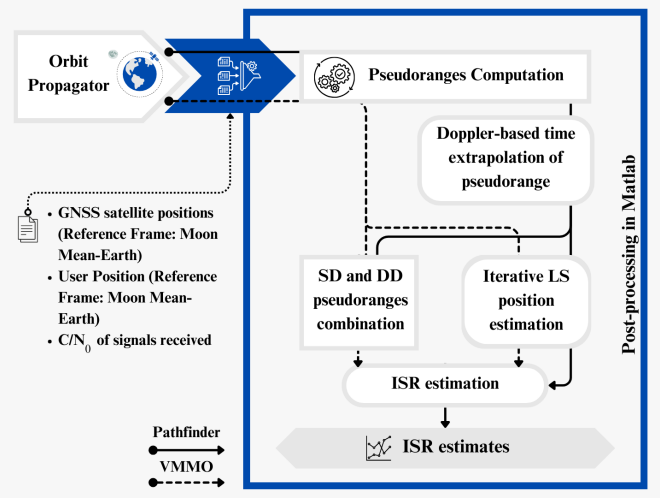

Fig. 2: Simulation blocks diagram.

In the post-processing stage, the C/N_0 are first converted to pseudorange standard deviations, providing an estimation of the code tracking accuracy as a function of the Radio-Frequency (RF) front end parameters and the C/N_0 [20]. These pseudorange measurements are created for each receiver at their respective measurements biased timestamps. This is done based on a realization of the pseudorange noise for a set number of Monte Carlo simulations. The pseudoranges of the aiding agent are then time extrapolated to align with the timestamps of the aided agent. Each aiding user's pseudorange measurement is extrapolated to its closest neighbor among the

aided user measurements' timestamps. The measurements rate of both receivers is considered to be 1 Hz, therefore each aiding agent's timestamp is assumed to have a neighbour at less than 0.5 s away. Therefore, an aiding agent measurement has to be time-extrapolated at most over a duration of 0.5 s. Once this process completed, the LS SPP estimates are obtained for each receiver. In parallel, the aided pseudorange measurements and the extrapolated aiding pseudorange measurements are passed through the pseudorange combination block to form the SD and DD quantities. These are then given to the ISR estimation block, together with the estimated SPP to estimate the ISR values for each Monte Carlo simulation, at each timestamp. The number of simulated datapoints then amounts to a total of $4 \times 60 \times 60 \times N_{MC} = 14400 \times N_{MC}$, where 4, the number of hours in the scenario, is multiplied by the number of seconds, since the sampling frequency is 1 Hz, and by N_{MC}, the number of Monte Carlo simulations. The number of Monte Carlo simulation run for this work is 100.

Fig. 3 depicts the selected lunar scenario, involving the cubesat VMMO mission orbiting the Moon in a Low Lunar Frozen Orbit (LLFO) orbit together with the Lunar Pathfinder, orbiting the Moon in a Elliptical Lunar Frozen Orbit (ELFO). Both missions were propagated in STK using the High-Precision Orbit Propagator (HPOP).

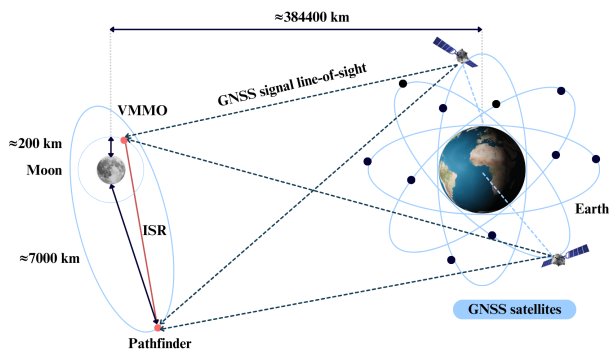

Fig. 3: Schematic of the GNSS scenario for VMMO and the Lunar Pathfinder. Not to scale.

The ISR truth and relative velocity is also given in Fig. 4 to support the statement that this analysis considers large baselines, and high relative dynamics.

Finally, a high-level overview of the settings considered to perform this simulation is provided in Table II.

IV. Results

In this section, the simulation results are presented, according to the methodology described in section III. First, the quality of the position estimated by the iterative LS algorithm is assessed, together with the quality of the ranging algorithms. Subsequently, the differential clock bias estimation obtained by the DGNSS ranging algorithm is shown and compared to the quality obtained by substracting the two individually estimated clock biases. Finally, the Doppler shift

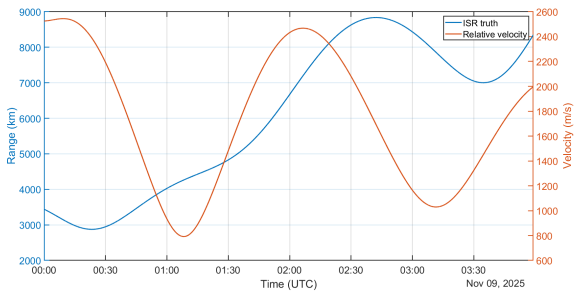

Fig. 4: ISR truth and relative velocity over the tested time window [9].

TABLE II: Scenario settings.

Parameter	Setting
GNSS	Galileo GPS
Frequency band	E5a-L5 (central frequency $f_c = 1176.45MHz$ and $\lambda = 0.2549\ m$)
Users	Pathfinder (ELFO) [6], [21] VMMO (polar LLFO) [22] Initial states propagated with HPOP [23]
Force model	Moon as central body (48, 48) Gravity file 'GL0660B.grv' [24] Earth-Sun as point masses
Receiver	Earth pointing antenna 14 dBi gain 15 dB-Hz sensitivity

values of the lunar user receiving terrestrial GNSS signals are presented, together with their rate to understand the effect of the large dynamics of such a DGNSS ranging scenario on the extrapolation of the pseudorange measurements.

A. DGNSS ranging performance in space

The quality of the position estimates obtained by a GNSS receiver orbiting the Moon with an iterative LS algorithm is presented in Fig. 5. The bias and standard deviation of the position error are presented for a set of 100 Monte Carlo simulations as specified in the section III. The error is presented in the 3D reference frame Moon-Mean Earth as defined in [25]. The particularity of this reference frame is that its x-axis is aligned with the Moon-Earth mean direction. This shows that estimated position uncertainty is largest in the direction from the lunar satellite to the Earth. This is because the GNSS signal directions as seen from the lunar orbit are clustered, making the position error in the line-of-sight direction and the clock bias error ambiguous. In order to show the effect of clock bias uncertainty on the DGNSS ranging algorithms, Fig. 6 shows the ISR performance in three different cases.

- Fig. 6a presents the Empirical Cumulative Distribution Function (ECDF) of the Root Mean Square Error (RMSE) in the case the two receivers are unrealistically perfectly synchronous with each other. In such a case, both the position estimation and the ISR are reduced to a 3D

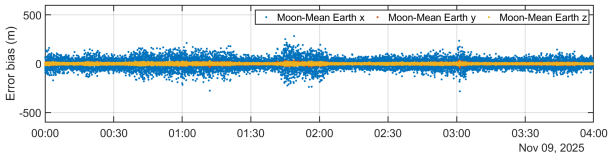

(a) LS 3D position error bias.

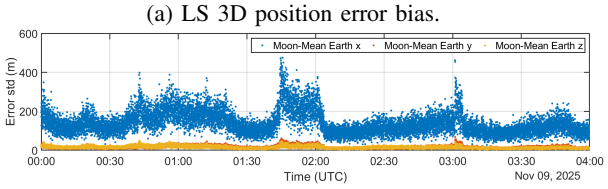

(b) LS 3D position error standard deviation.

Fig. 5: Error on the LS estimated position of VMMO.

problem as the clock biases are assumed to be zero and known in advance. In that situation, the range between a pair of lunar receivers can be estimated with DGNSS ranging with an RMSE below 10 m at all times, as shown by the APD, the SD H_{ideal} and SD $H_{aided,corrected}$ techniques, introduced in Table I. It is also to be noted that the algorithms suggested as more adequate for the lunar DGNSS scenario present RMSE values from 1 to 4 orders of magnitude lower when compared to the DGNSS algorithm used in the terrestrial applications.

- In the second case, the receivers measurements are considered asynchronous. In that case, the positioning problem comes back to a 4D problem to estimate the 3D position and the local clock bias of each receiver. The estimated clock bias from the first stage is then used to correct the pseudorange measurements such that the ISR SD problem can be still treated as a 3D problem. This analysis shows that the ISR estimates are significantly affected by the time uncertainty due to the error on the clock bias estimation. Indeed, the RMSE of the most accurate techniques among those presented worsens by at least one order of magnitude as shown in Fig. 6b. It is also interesting to note that, if the common terrestrial DGNSS ranging algorithm is applied to the geometry of lunar orbiters instead, the maximum RMSE remains unchanged when compared to the first scenario. The geometry bias caused by the invalid parallelism assumption is indeed dominant in that case.
- Finally, in the third scenario, the receivers are also considered asynchronous but this time the pseudorange measurements are given raw to the ISR estimation stage. The SD ISR estimation hence becomes a 4D problem as the differential clock bias also has to be estimated. The results of this analysis presented in Fig. 6c show that the ranging performance of the SD algorithm worsens and becomes similar to those of the DD algorithms. The ISR ranging estimation bias hence increases when the SD algorithm is 4D. The DD algorithms ranging performance remain unchanged over all the scenarios as the differential clock biases (or the differential residual errors on the prior estimation of the clock bias in the second scenario) are cancelled during the combinations of two SDs to two different GNSS satellites.

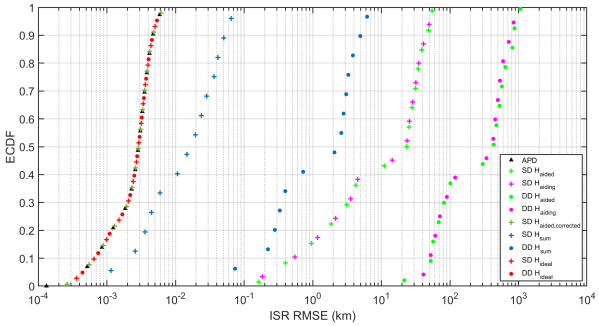

(a) Synchronous receivers. LS and ISR estimations 3D.

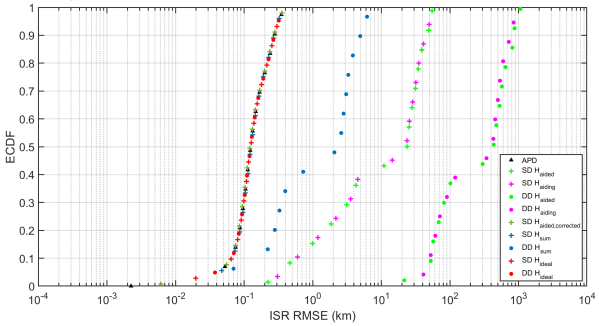

(b) Asynchronous receivers. LS 4D and ISR estimation 3D.

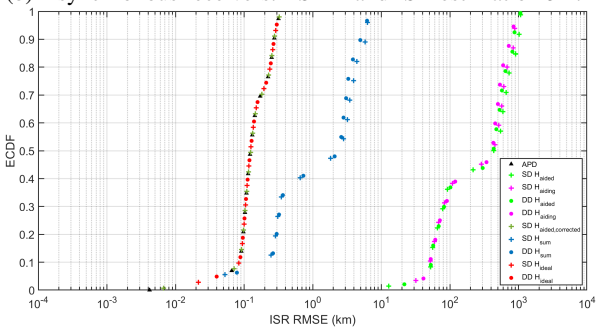

(c) Asynchronous receivers. LS and ISR estimations 4D.

Fig. 6: ISR estimates quality for different hypotheses of the receivers' time knowledge.

B. DGNSS differential clock bias estimation in space

In this section, the quality of the differential clock bias estimated by the DGNSS SD algorithm is assessed and compared to the quality of the difference of estimated clock biases, as defined in section II-D. This is presented in the form of a boxplot to depict the time evolution of the Probability Density Function (PDF) of the estimation errors over the Monte Carlo simulations in Fig. 7. Fig. 7a shows the estimation quality of the clock bias of VMMO obtained by the iterative LS estimator. It shows that at all times over the $4h$ simulated data, 50% of the estimations present an error lower than $0.8\,\mu$s. This value increases slightly up to 1 μs for the difference of estimated clock biases, as observed in Fig. 7b. Also,

the variance increases as shown by the whiskers expanding further in Fig. 7b. The performance of the difference of estimated clock biases proves similar to those estimated by the DGNSS SD algorithm presented in Fig. 7c. These values are also coherent with the Time Dilution of Precision (TDOP) calculated from the respective design matrices.

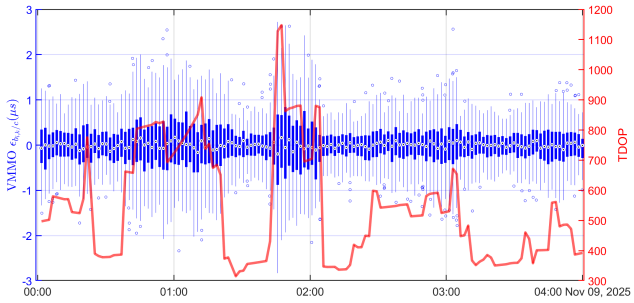

(a) VMMO estimated clock bias error.

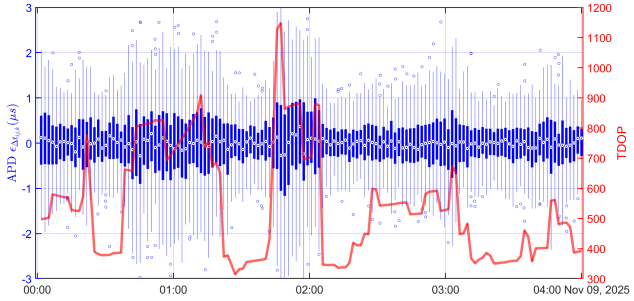

(b) Difference of estimated clock biases.

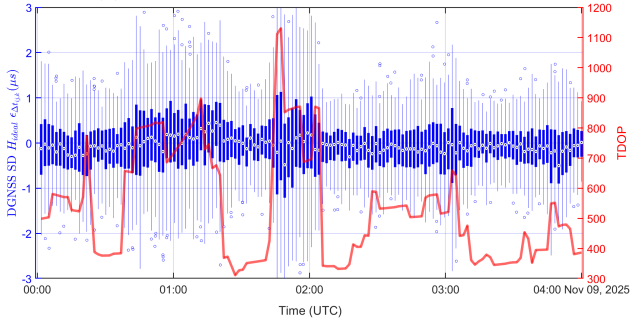

(c) ISR SD ranging differential clock bias.

Fig. 7: Boxplot of the time evolution of the PDF of the VMMO estimated clock bias error (a) and the estimated differential clock bias error for the different methods (b and c).

C. Effect of the large dynamics on the time-extrapolation of the pseudorange measurements

Finally, the current analysis aims to assess the impact the large dynamics inherent in a lunar DGNSS scenario could have on the time-extrapolation of the pseudorange measurements, being a necessary step to combine asynchronous measurements. To this end, Fig. 8 shows the Doppler shifts between the Lunar Pathfinder mission and the terrestrial GNSS satellites over time. These values are about 10 times larger than those of a terrestrial GNSS user. Despite being large, the largest value would not impact much the Doppler-based time extrapolation performance. Indeed, if we consider the APD technique to estimate the differential clock bias, of which the error is presented in Fig. 7b, the error has 50% probability to be lower than $1\ \mu s$ at all times of the simulated window, this value multiplied by the upper bound of Doppler shifts in this simulation, $20\ kHz$, and the wavelength of $E5a/L5$ carrier frequency, $0.2549\ m$, as per (5), represents an extrapolation error of $5\ mm$. Moreover, the Doppler shifts variations are still relatively limited in range as shown in Fig. 8b. Indeed, over the simulated period, the Doppler rates remain below $2\ Hz/s$, which, in terms of effect it can have on the time-extrapolation technique of the pseudorange measurements, remains low. Indeed, as described in section III, two receivers with a measurements rate of $1\ Hz$ might have to combine measurements at most $0.5\ s$ apart. This means that the pseudoranges of the aiding user should be extrapolated over a maximum of $0.5\ s$. If we consider the maximum Doppler rate value of $2\ Hz/s$, this would correspond to a change of $1\ Hz$ over $0.5\ s$, hence to a pseudorange variation of $0.2549\ m$ (for the $E5a/L5$ band), considered as negligible in the space GNSS context. The effect that the noise affecting Doppler shifts instead is ignored, as it would be multiplied only by a small factor of $\lambda_{f_c} \times \Delta t_{ij,k} = 0.2549 \times 0.5 = 0.127$, at worst, which is considered negligible in the lunar GNSS context.

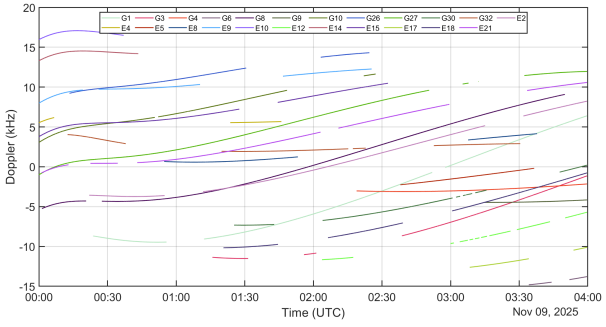

(a) Doppler.

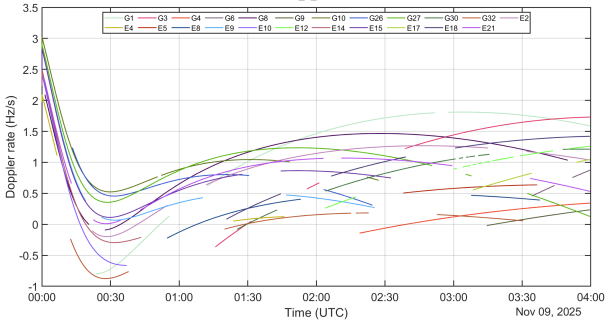

(b) Doppler rate.

Fig. 8: Doppler and Doppler rate between a lunar orbiter (Pathfinder) and the GNSS satellites (Galileo and GPS).

V. CONCLUSION

The present contribution analyses and presents the performance of differential GNSS ranging and differential clock

bias estimation in space. In particular, it assesses the cooperation between two lunar orbiters, both receiving Galileo and GPS signals from terrestrial constellations. Their GNSS receiver makes pseudorange and Doppler measurements at 1 Hz, based on their respective onboard local clock, leading their measurements to be asynchronous. The measurements of the aiding user are first time-extrapolated to compensate for the measurements time offset between the two receivers. The combination of these measurements is then performed through SDs and DDs and subsequently used to compute both the ISR as well as their differential clock bias. The results confirm that the traditional terrestrial ranging DGNSS algorithm is outperformed by updated algorithms to adapt for the large baseline characterizing a pair of lunar orbiters receiving GNSS signals from terrestrial constellations. The significant effect of noisy clock biases estimation on the ranging performance is observed. However, the large dynamics of such scenarios translated into large Doppler shifts of GNSS signals do not appear to cause significant Doppler-based time extrapolation error. This analysis provides an informative background to further improve the potential performance of DGNSS ranging in space and eventually benefit from its potential of common correlated errors cancellation on the combined GNSS measurements.

ACKNOWLEDGMENT

This work has been performed under the ESA Contract No. 4000134565/21/NL/GLC/my that is co-funding the PhD grant of Ms. Anaïs Delépaut. The content of the present article reflects solely the authors' view and by no means represents the official view of the European Space Agency (ESA). In any reproduction of this article, there should not be any suggestion that ESA or this article endorses any specific organisation or products. The use of the ESA logo is not permitted. This notice should be preserved along with the article's original URL.

REFERENCES

[1] A. Delépaut, P. Giordano, J. Ventura-Traveset, D. Blonski, M. Schönfeldt, P. Schoonejans, S. Aziz, and R. Walker, "Use of GNSS for lunar missions and plans for lunar in-orbit development," *Advances in Space Research*, vol. 66, no. 12, pp. 2739–2756, 2020.

[2] SpacePNT, "SpacePNT: NaviMoon," https://spacepnt.com/navimoon/, 2023.

[3] V. Capuano, P. Blunt, C. Botteron, and P.-A. Farine, "Orbital filter aiding of a high sensitivity GPS receiver for lunar missions," *NAVIGATION, Journal of the Institute of Navigation*, vol. 64, no. 3, pp. 323–338, 2017.

[4] J. J. Parker, F. Dovis, B. Anderson, L. Ansalone, B. Ashman, F. H. Bauer, G. D'Amore, C. Facchinetti, S. Fantinato, G. Impresario *et al.*, "The Lunar GNSS Receiver Experiment (LuGRE)," in *Proceedings of the 2022 International Technical Meeting of The Institute of Navigation*, 2022, pp. 420–437.

[5] ASI, "LuGRE sets another record: first GNSS signals detected in lunar orbit," https://www.asi.it/en/2025/02/lugre-sets-another-record-first-gnss-signals-detected-in-lunar-orbit/, 2025.

[6] Surrey Satellite Technology Ltd, "Lunar Pathfinder," https://www.sstl.co.uk/space-portfolio/missions-in-build/2022/lunar-pathfinder, 2023.

[7] E. D. Kaplan and C. Hegarty, *Understanding GPS/GNSS: principles and applications*. Artech House, 2017.

[8] A. Jones, "Europe launches ambitious 'Moonlight' program to support lunar exploration," https://www.space.com/europe-moonlight-program-lunar-navigation-communications, 2024.

[9] A. Delépaut, A. Minetto, and F. Dovis, "Code-Based Differential GNSS Ranging for Lunar Orbiters: Theoretical Review and Application to the NaviMoon Observables," *Remote Sensing*, vol. 16, no. 15, 2024.

[10] A. Delépaut, A. Minetto, F. Dovis, F. Melman, P. Giordano, and J. Ventura-Traveset, "Enhanced GNSS-based positioning in space exploiting inter-spacecraft cooperation," in *Proceedings of the 2022 International Technical Meeting of The Institute of Navigation*, 2022, pp. 530–544.

[11] F. de Ponte Müller, A. Steingass, and T. Strang, "Zero-baseline measurements for relative positioning in vehicular environments," in *Proceedings of the 6th European Workshop on GNSS Signals and Signal Processing of Universität der Bundeswehr*, 2013.

[12] M. Tahir, S. S. Afzal, M. S. Chughtai, and K. Ali, "On the accuracy of inter-vehicular range measurements using GNSS observables in a cooperative framework," *IEEE Transactions on Intelligent Transportation Systems*, pp. 1–10, Jun. 2018.

[13] J. S. Subirana, J. Zornoza, and M. Hernández-Pajares, *GNSS DATA PROCESSING*. ESA Communications, 2013, vol. I: Fundamentals and Algorithms.

[14] P. J. Teunissen and O. Montenbruck, *Springer handbook of global navigation satellite systems*. Springer, 2017, vol. 10.

[15] R. B. Langley, "Gps receiver system noise," *GPS world*, vol. 8, no. 6, pp. 40–45, 1997.

[16] Y. Cai, Y. Li, and Z. Wang, "Real-time high-precision baseline measurement of satellite formation flying based on GNSS," *Advances in Space Research*, 2024.

[17] A. Minetto, G. Ammirante, F. Stesina, F. Dovis, and S. Corpino, "DGNSS ranging for cubesat rendezvous and docking manoeuvres at leo," in *2023 IEEE 10th International Workshop on Metrology for AeroSpace (MetroAeroSpace)*. IEEE, 2023, pp. 597–602.

[18] W. Yang, Y. Liu, and F. Liu, "An improved relative GNSS tracking method utilizing single frequency receivers," *Sensors*, vol. 20, no. 15, p. 4073, 2020.

[19] U. Tancredi, A. Renga, and M. Grassi, "Real-time relative positioning of spacecraft over long baselines," *Journal of Guidance, Control, and Dynamics*, vol. 37, no. 1, pp. 47–58, 2014.

[20] J. W. Betz and P. B. Fine, "Effect of narrow correlator spacing on code tracking accuracy," in *Proceedings of the 2000 National Technical Meeting of the Institute of Navigation*, 2000, pp. 716–723.

[21] Surrey Satellite Technology Ltd, "Lunar Pathfinder Data relay satellite in orbit around the Moon," https://www.sstl.co.uk/getmedia/690f1da3-a935-4c4d-b48c-616ac8417cb1/LunarPathfinder-UserManual-WebSite-v003.pdf, 2020.

[22] N. Database, "VMMO (Volatile and Mineralogy Mapping Orbiter)," https://www.nanosats.eu/sat/vmmo, 2025.

[23] AGI, "STK: High-Precision Orbit Propagator (HPOP)," https://help.agi.com/stk/11.4.1/, 2018.

[24] A. S. Konopliv, R. S. Park, D.-N. Yuan, S. W. Asmar, M. M. Watkins, J. G. Williams, E. Fahnestock, G. Kruizinga, M. Paik, D. Strekalov *et al.*, "The JPL lunar gravity field to spherical harmonic degree 660 from the GRAIL Primary Mission," *Journal of Geophysical Research: Planets*, vol. 118, no. 7, pp. 1415–1434, 2013.

[25] AGI, "Descriptions of Coordinate Systems in STK," https://help.agi.com/stk/11.4.1/, 2018.